Elia Turco, Shantanu Mishra, Jason Melidonie, Kristjan Eimre, Sebastian Obermann, Carlo A. Pignedoli, Roman Fasel, Xinliang Feng, and Pascal Ruffieux

On-Surface Synthesis and Characterization of Super-nonazethrene

J. Phys. Chem. Lett. 12, 8314–8319 (2021)

https://doi.org/10.1021/acs.jpclett.1c02381

On-Surface Synthesis and Characterization of Super-Nonazethrene

Elia Turco,[⊥,‡] Shantanu Mishra,[⊥,‡,†,*] Jason Melidonie,[‖,‡] Kristjan Eimre,[⊥] Sebastian Obermann,[‖] Carlo A. Pignedoli,[⊥] Roman Fasel,[⊥,§] Xinliang Feng,[‖,○,*] and Pascal Ruffieux[⊥,*]

[⊥]nanotech@surfaces laboratory, Empa – Swiss Federal Laboratories for Materials Science and Technology, 8600 Dübendorf, Switzerland

[‖]Faculty of Chemistry and Food Chemistry, and Center for Advancing Electronics Dresden, Technical University of Dresden, 01069 Dresden, Germany

[○]Department of Synthetic Materials and Functional Devices, Max Planck Institute of Microstructure Physics, 06120 Halle, Germany

[§]Department of Chemistry, Biochemistry and Pharmaceutical Sciences, University of Bern, 3012 Bern, Switzerland

AUTHOR INFORMATION

Corresponding Authors

[*]Shantanu Mishra – Empa − Swiss Federal Laboratories for Materials Science and Technology, 8600 Dübendorf, Switzerland; orcid.org/0000-0002-2900-4203; Email: shantanu.mishra@empa.ch

[*]Xinliang Feng – Faculty of Chemistry and Food Chemistry, and Center for Advancing Electronics Dresden, Technical University of Dresden, 01069 Dresden, Germany; Department of Synthetic Materials and Functional Devices, Max Planck Institute of Microstructure Physics, 06120 Halle, Germany; orcid.org/0000-0003-3885-2703; Email: xinliang.feng@tu-dresden.de

[*]Pascal Ruffieux – Empa − Swiss Federal Laboratories for Materials Science and Technology, 8600 Dübendorf, Switzerland; orcid.org/0000-0001-5729-5354; Email: pascal.ruffieux@empa.ch

Present Addresses

[†]Shantanu Mishra – IBM Research – Zurich, 8803 Rüschlikon, Switzerland

Author Contributions

[‡]These authors contributed equally

Zethrenes and their laterally-extended homologues, super-zethrenes, have been intensively studied in the solution phase, and widely investigated as optical and charge transport materials. Super-zethrenes are also considered to exhibit an open-shell ground state, and may thus serve

as model compounds to investigate nanoscale π-magnetism. However, their synthesis is extremely challenging due to their high reactivity. We report here the on-surface synthesis of the hitherto largest zethrene homologue, super-nonazethrene, on Au(111). Using single-molecule scanning tunneling microscopy and spectroscopy, we show that super-nonazethrene exhibits an open-shell singlet ground state featuring a large spin polarization-driven electronic gap of 1 eV. High-resolution tunneling spectroscopy further reveals singlet-triplet spin excitations in super-nonazethrene, characterized by a strong intramolecular exchange coupling of 51 meV. Given the paucity of zethrene chemistry on surfaces, our results therefore provide unprecedented access to large open-shell zethrene compounds amenable to scanning probe measurements, with potential application in molecular spintronics.

TOC Graphic

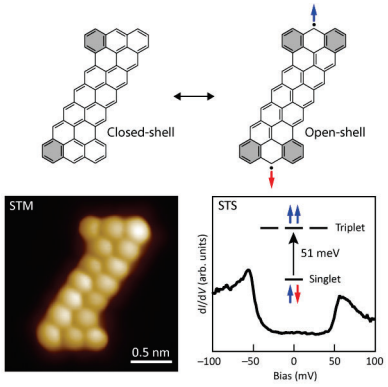

KEYWORDS: Scanning tunneling microscopy, scanning tunneling spectroscopy, polycyclic aromatic hydrocarbons, molecular magnetism, electronic structure, on-surface synthesis

Polycyclic aromatic hydrocarbons (PAHs) display a range of physico-chemical properties of both fundamental interest and technological relevance, which is highly tunable through variations in molecular size, shape and edge structure. For example, while PAHs with armchair edges are generally stable with large HOMO-LUMO (highest occupied molecular orbital-lowest unoccupied molecular orbital) gaps; PAHs with zigzag edges are more reactive, feature relatively smaller HOMO-LUMO gaps and may exhibit open-shell (magnetic) ground states. This opens extensive opportunities in molecular electronics, non-linear optics and quantum computation.[1,2] However, synthesis of open-shell PAHs in solution poses significant challenges due to their high intrinsic reactivity. Alternatively, open-shell PAHs can be synthesized and stabilized on solid surfaces via on-surface synthesis[3] under ultra-high vacuum. This approach additionally allows in-situ single-molecule chemical, electronic and magnetic characterization using scanning tunneling microscopy (STM) and spectroscopy (STS).

Lately, on-surface synthesis has been utilized to synthesize a number of PAHs with zigzag edges, such as acenes,[4–7] periacenes,[8–10] anthenes,[11] periacenoacenes,[12] triangulenes[13–19] and Clar's goblet,[20] with many of them featuring an open-shell ground state. Another prominent

class of open-shell PAHs are zethrenes,[21] which are Z-shaped PAHs with mixed zigzag and armchair edges (Scheme 1). While the parent zethrene (first reported by Clar et al.[22]) is closed-shell, longitudinal extension of zethrenes generates proaromatic quinodimethane moieties which tend to promote an open-shell ground state, as has been demonstrated through the syntheses of the derivatives of heptazethrene[23] to nonazethrene.[24] It has also been shown theoretically[24] that compared to acenes, to which they are closely related, zethrenes exhibit a faster increase of radical character and a faster decrease of singlet-triplet gap with increasing number of benzenoid rings. Furthermore, lateral extension of zethrenes leads to the so-called super-zethrene compounds, which are considered to be inherently open-shell.[21] While the parent super-zethrene has not been realized, solution syntheses of the larger homologues, *viz.* derivatives of super-heptazethrene[25] and super-octazethrene,[26] have been recently reported. The rich chemistry of zethrenes in the solution phase is in contrast to on-surface synthesis of zethrenes, which has largely remained unexplored. Only last year, we reported the synthesis of unsubstituted super-heptazethrene on Au(111),[27] which was found to exhibit a closed-shell ground state. Access to larger zethrenes should therefore not only offer the possibility of investigating unconventional π-magnetism at the single molecule scale, but also enable potential application of zethrenes in molecular electronics and optics, for example, as building blocks for high-mobility graphene nanoribbons and graphene nanoribbon-based spin filter devices,[28] and organic near-infrared dyes.[21] Here, we report a combined in-solution and on-surface synthesis of the hitherto largest zethrene compound – unsubstituted super-nonazethrene (**1**), and its atomic-scale characterization on an inert Au(111) surface. In particular, our bond-resolved STM[29,30] and STS measurements conclusively demonstrate that **1** exhibits an open-shell ground state with an intramolecular magnetic exchange coupling of 51 meV.

Scheme 1. (a) Closed-shell Kekulè and open-shell non-Kekulè resonance structures of zethrenes and super-zethrenes, and their structural relationship to the parent zethrene. (b) Combined in-solution and on-surface synthetic route toward 1.[a,b]

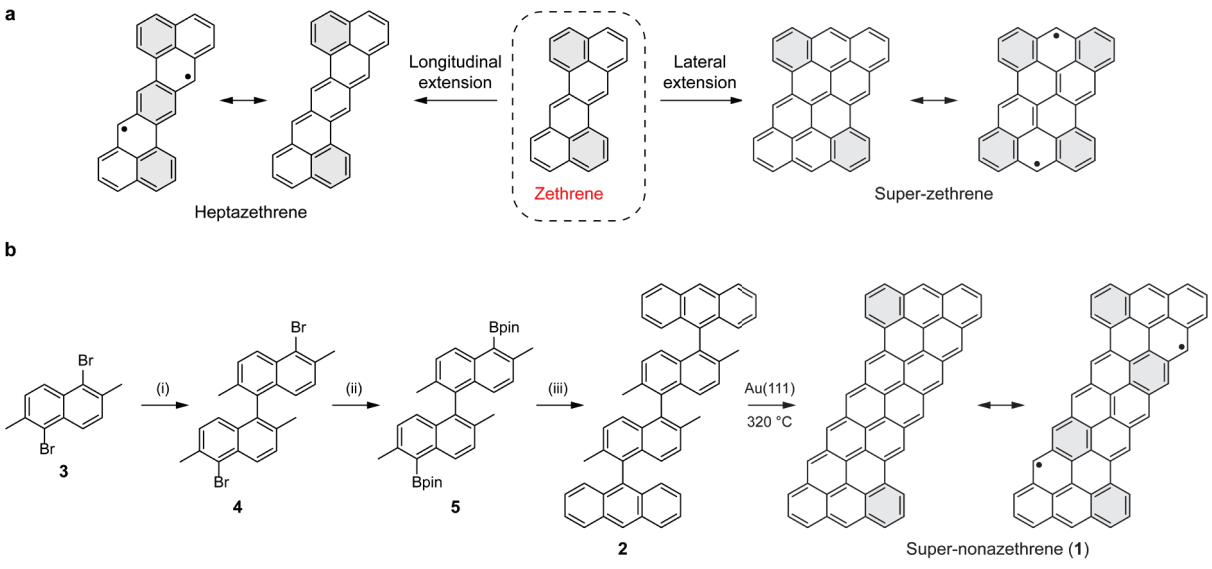

[a]Filled rings denote Clar sextets. [b]Reagents and conditions: (i) *n*-BuLi, $CuCl_2$, THF, –78 °C to room temperature, 18 h, 58%; (ii) KOAc, $(Bpin)_2$, $Pd(dppf)Cl_2$, DMSO, 80 °C, 20 h, 99%; and (iii) 9-bromoanthracene, K_3PO_4, $Pd_2(dba)_3$, DPEPhos, PhMe/EtOH/H_2O, 110 °C, 3 d, 39%.

To synthesize **1**, we designed the precursor 9,9'-(2,2',6,6'-tetramethyl-[1,1'-binaphthalene]5,5'diyl) dianthracene (**2**), which undergoes thermally induced cyclodehydrogenation and oxidative cyclization of methyl groups on a metal surface (Scheme 1). The synthesis of **2** started with the treatment of 1,5-dibromo-2,6-dimethylnaphthalene (**3**)[31] with *n*-BuLi and $CuCl_2$ at –78 °C, which provided the dimer 5,5'-dibromo-2,2',6,6'-tetramethyl-1,1'-binaphthalene (**4**) in good yield.[32] In a next step, 2,2'-(2,2',6,6'-tetramethyl-[1,1'-binaphthalene]-5,5'-diyl)bis(4,4,5,5-tetramethyl-1,3,2-dioxaborolane) (**5**) was obtained under Suzuki–Miyaura conditions in quantitative yield using [1,1'-bis-(diphenylphosphino)ferrocene]dichloropalladium(II) dichloride as the catalyst, potassium acetate as the base and bis(pinacolato)diboron ($(Bpin)_2$) as the borylation reagent.[33] Finally, anthracene substituents were introduced to **5** through the Suzuki reaction, leading to the formation of **2** in 39% yield under the catalysis of tris(dibenzylideneacetone)dipalladium(0) ($Pd_2(dba)_3$) and bis[(2-diphenylphosphino)-phenyl]ether (DPEPhos).[34]

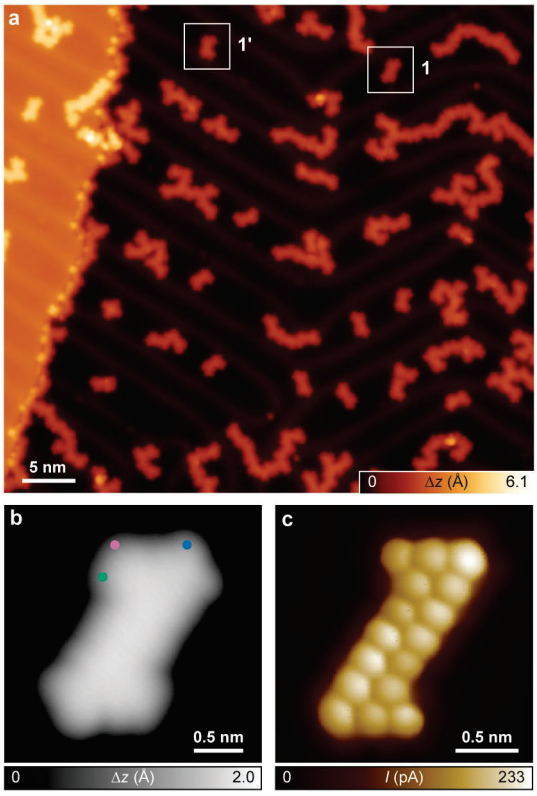

Figure 1. (a) Overview STM image after annealing **2** on Au(111) at 320 °C (V = –0.7 V, I = 70 pA). **1** and **1'** are highlighted. (b, c) High-resolution STM image (b) (V = –0.1 V, I = 50 pA) and corresponding bond-resolved STM image (c) (V = –5 mV, I = 50 pA, Δh = –0.8 Å) of **1** on Au(111), acquired with a carbon monoxide (CO) functionalized tip.

A submonolayer coverage of **2** was sublimed on a Au(111) surface held at room temperature, and the surface was annealed to 320 °C to promote the on-surface reactions. Subsequent STM imaging of the surface revealed covalently coupled molecular clusters as the predominant species (~80%) along with a minority of individual molecules (~20%) (Fig. 1a). High-resolution STM imaging showed that ~22% of the individual molecules present a uniform Z-shaped topography consistent with **1** (Fig. 1b), which is confirmed via bond-resolved STM imaging (Fig. 1c), thereby demonstrating the success of our synthetic strategy. We note that the remaining 78% of individual molecules consist of partially reacted precursor molecules, and an isomer of **1**, referred to as **1'**, which is formed by a 180° rotation of one of the 9-(2,6-dimethylnaphthalen-1-yl)anthracene moieties of **2** relative to the other, and its subsequent cyclodehydrogenation and oxidative cyclization (Fig. S1). The low yield of individual molecules on Au(111) in the present case (~20%), is in marked contrast with our previously reported synthesis of super-heptazethrene on Au(111)[27] with an 82% yield of individual molecules under similar reaction conditions, which likely arises from the open-shell ground states[12] of **1** and **1'**, as we demonstrate below. With the aim of increasing the yield of **1**, we also explored its synthesis on the more active Ag(111) and Cu(111) surfaces (Fig. S2), where however the absolute yields of **1** remained below 10%.

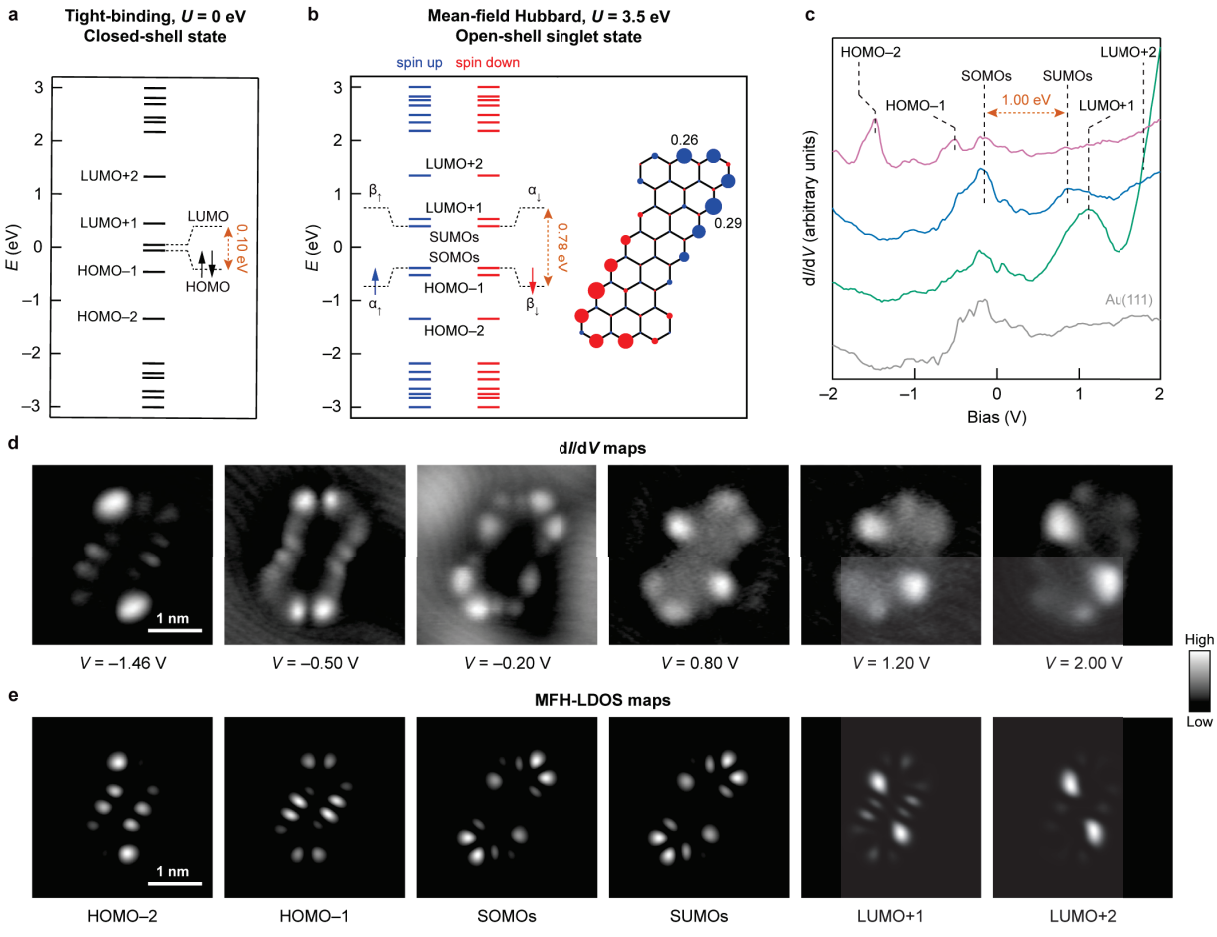

Figure 2. (a, b) Nearest-neighbor TB (a) and MFH (b) energy spectrum of **1**. *U* denotes the on-site Coulomb repulsion. Also shown is the spin polarization plot of **1**, where blue and red filled circles denote mean populations

of spin up and spin down electrons, respectively, and the numbers denote the two largest mean populations of spin up electrons. (c) dI/dV spectroscopy on **1** revealing molecular orbital resonances (open feedback parameters: V = –2.0 V, I = 350 pA; V_{rms} = 16 mV). Acquisition positions are indicated in Fig. 1b. (d) Constant-current dI/dV maps at the resonances indicated in (c) (I = 300–320 pA; V_{rms} = 30 mV). (e) MFH-LDOS maps of the HOMO–2 to LUMO+2 of **1**.

To study the electronic structure of **1**, we start by performing nearest-neighbor tight-binding (TB) calculations, which do not involve electron-electron interactions necessary to describe magnetism, and therefore lead to a closed-shell state of **1**. Figure 2a shows the TB energy spectrum of **1**, where the principal features are a pair of frontier states located close to zero energy that correspond to the HOMO and LUMO, with the corresponding wave functions localized at the zigzag termini of **1** (Fig. S3 and S4). The calculated HOMO-LUMO gap of **1** is 0.10 eV. Next, we perform mean-field Hubbard (MFH) calculations accounting for electron-electron interactions, which lead to spin polarization of **1**. The frontier electronic structure is now characterized by a pair of singly occupied molecular orbitals (SOMOs) α and β (Fig. 2b), with an antiferromagnetic correlation of the populating spins (that is, an open-shell singlet ground state, see Fig. S5), in accordance with Ovchinnikov's rule.[35] The calculated wave functions of SOMOs and the associated unoccupied orbitals (SUMOs) exhibit a largely disjoint character, as is expected for an open-shell singlet diradicaloid (Fig. S6 and S7). Spin polarization of **1** results in a significant opening of the frontier gap with the calculated SOMO-SUMO gap being 0.78 eV.

We employed STS to probe the experimental electronic structure of **1**. dI/dV spectroscopy on **1** (where I and V denote the tunneling current and bias voltage, respectively) reveals six distinguishable features in the local density of states (LDOS) at –1.46 V, –0.50 V, –0.20 V, 0.80 V, 1.20 V and around 1.80 V (Fig. 2c). Corresponding dI/dV maps at –1.46 V, –0.50 V, 1.20 V and 2.00 V (Fig. 2d) exhibit a good match with the calculated MFH-LDOS maps of the HOMO–2, HOMO–1, LUMO+1 and LUMO+2 of **1**, respectively (Fig. 2e). Furthermore, the frontier orbital dI/dV maps at –0.20 V and 0.80 V show similar shapes and LDOS symmetries, which suggests that at –0.20 V/0.80 V, electron tunneling from/to singly occupied orbitals are involved. The dI/dV maps at –0.20 V and 0.80 V agree well with the MFH-LDOS maps of the SOMOs and SUMOs of **1**, which supports an open-shell ground state of **1**. In addition, we note that the frontier electronic gap of **1** on Au(111) is 1.00 eV, which is much larger than the HOMO-LUMO gap of 0.23 eV of super-heptazethrene on Au(111).[27] Given that the HOMO-LUMO gap of a homologous series of molecules should decrease with increasing molecular size, the counterintuitive increase of the frontier electronic gap of **1** compared to its smaller homologue super-heptazethrene therefore cannot be explained by a closed-shell ground state of **1**. Specifically, Fig. S4 shows the evolution of the HOMO-LUMO gaps of zethrenes and superzethrenes in the absence of Coulomb correlations, where the gaps clearly decrease with increasing system size for both species. This strongly suggests that the electronic gap of **1** corresponds to a spin polarization-driven Coulomb gap and the frontier states correspond to SOMOs. Our

interpretation is supported by spin-polarized density functional theory calculations on **1**, which yield the open-shell singlet as the ground state of **1**, with the open-shell triplet and the closed-shell states 53 meV and 0.12 eV higher in energy, respectively (Fig. S8). Furthermore, for both the open-shell singlet and closed-shell states of **1**, we performed eigenvalue self-consistent GW+IC calculations, which include screening effects from the Au(111) surface (Fig. S8). From our calculations, the experimental frontier gap of 1.00 eV is consistent with the GW+IC gap of 0.70 eV for the open-shell singlet state of **1**, while clearly disagreeing with the GW+IC gap of 90 meV for the closed-shell state of **1**, which thus confirms the open-shell ground state of **1** on Au(111). We note that other possible origins of the reopening of the frontier gap from super-heptazethrene to **1**, such as hybridization of molecular orbitals of **1** with the underlying Au surface, can be discarded based on two reasons: (1) the planar adsorption configuration of **1** on Au(111) seen from STM imaging (Fig. 1c) indicates an absence of chemical bonding to the surface, and (2) there is no evidence of charge transfer between **1** and the Au surface, as the frontier molecular orbitals of **1** are detected far from the Fermi energy and at the expected bias polarities.

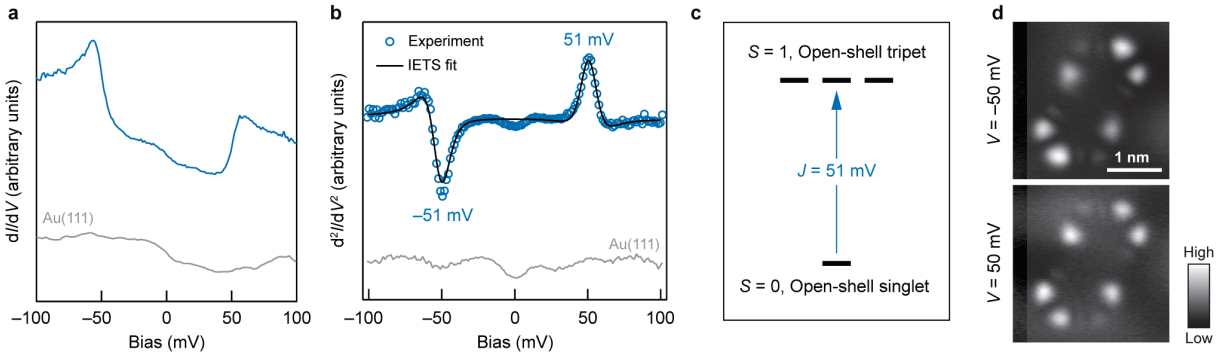

Figure 3. (a, b) dI/dV (a) and d^2I/dV^2 (b) spectrum acquired on **1**, revealing singlet-triplet spin excitations (open feedback parameters: V = –100 mV, I = 1.2 nA (a) and 2.0 nA (b); V_{rms} = 400 µV (a) and 4 mV (b)). Acquisition position is indicated in Fig. 1b. Also shown is an inelastic electron tunneling spectroscopy (IETS) fit to the d^2I/dV^2 spectrum using a spin-½ Heisenberg dimer model, which yields the spin excitation threshold as 51 mV. (c) Schematic representation of the spin excitation. (d) Constant-current dI/dV maps near the spin excitation threshold (I = 280 pA; V_{rms} = 4 mV).

A final and direct experimental proof of the open-shell ground state of **1** comes from low-bias dI/dV spectroscopy on **1** that reveals conductance steps symmetric about the Fermi energy, which correspond to inelastic excitations[36] (Fig. 3a,b). Given that their occurrence is concurrent with the observation of SOMOs, we attribute these inelastic excitations to singlet-triplet spin excitations (Fig. 3c).[20,37–39] In this picture, tunneling electrons may cause spin excitation of a coupled spin system whenever their energy e$V \geq J$, where J denotes the magnetic exchange coupling of the radicals in **1**, or equivalently, the singlet-triplet gap of **1**. The excitation threshold, extracted from a fit to the experimental d^2I/dV^2 spectrum with a spin-½ Heisenberg dimer model,[39] amounts to 51 meV (Fig. 3b). The spatial distribution of the spin excitation

signal is visualized through acquisition of dI/dV maps around the spin excitation threshold (Fig. 3d), which resemble the SOMOs/SUMOs LDOS.

In summary, we have successfully synthesized unsubstituted and stable super-nonazethrene on Au(111). We employ STM and STS measurements at submolecular resolution to probe the chemical, electronic and magnetic structure of **1**. Comparison of our experimental STS data with theoretical calculations provides conclusive evidence of the open-shell singlet ground state of **1**. Low-bias STS measurements reveal singlet-triplet spin excitations in **1**, with the corresponding singlet-triplet gap being 51 meV, exceeding the room temperature thermal energy (25.7 meV at 298 K) by almost a factor of two. Our results provide crucial insights into the emergence of robust π-magnetism in PAHs, with implications in low-dimensional magnetism and organic spintronics.

ASSOCIATED CONTENT

Supporting Information

The Supporting Information is available free of charge at https://pubs.acs.org/.

Detailed synthetic description of chemical compounds reported in this study and associated solution characterization data, additional STM and STS data, additional calculations, and experimental and calculation methods (PDF).

Notes

The source data for the results presented in this work is publicly accessible from the Materials Cloud platform (DOI: 10.24435/materialscloud:j7-51).

The authors declare no competing financial interest.

ACKNOWLEDGEMENTS

This work was supported by the Swiss National Science Foundation (grant no. 200020-182015 and IZLCZ2-170184), the NCCR MARVEL funded by the Swiss National Science Foundation (grant no. 51NF40-182892), the EU Horizon 2020 research and innovation program – Marie Skłodowska-Curie grant no. 813036 and Graphene Flagship Core 3 (grant no. 881603), the Office of Naval Research (grant no. N00014-18-1-2708), ERC Consolidator grant (T2DCP, no. 819698), and the German Research Foundation within the Cluster of Excellence – Center for Advancing Electronics Dresden and EnhanceNano (grant no. 391979941). Computational support from the Swiss National Supercomputing Centre under project ID s904 is acknowledged.

REFERENCES

(1) Yazyev, O. V. Emergence of Magnetism in Graphene Materials and Nanostructures. *Rep. Prog. Phys.* **2010**, *73*, 056501.

(2) Das, S.; Wu, J. Polycyclic Hydrocarbons with an Open-Shell Ground State. *Phys. Sci. Rev.* **2017**, *2*, 20160109.

(3) Clair, S.; de Oteyza, D. G. Controlling a Chemical Coupling Reaction on a Surface: Tools and Strategies for On-Surface Synthesis. *Chem. Rev.* **2019**, *119*, 4717–4776.

(4) Urgel, J. I.; Mishra, S.; Hayashi, H.; Wilhelm, J.; Pignedoli, C. A.; Giovannantonio, M. D.; Widmer, R.; Yamashita, M.; Hieda, N.; Ruffieux, P.; Yamada, H.; Fasel, R. On-Surface Light-Induced Generation of Higher Acenes and Elucidation of Their Open-Shell Character. *Nat. Commun.* **2019**, *10*, 1–9.

(5) Krüger, J.; García, F.; Eisenhut, F.; Skidin, D.; Alonso, J. M.; Guitián, E.; Pérez, D.; Cuniberti, G.; Moresco, F.; Peña, D. Decacene: On-Surface Generation. *Angew. Chem. Int. Ed.* **2017**, *56*, 11945–11948.

(6) Zuzak, R.; Dorel, R.; Kolmer, M.; Szymonski, M.; Godlewski, S.; Echavarren, A. M. Higher Acenes by On-Surface Dehydrogenation: From Heptacene to Undecacene. *Angew. Chem. Int. Ed.* **2018**, *57*, 10500–10505.

(7) Eisenhut, F.; Kühne, T.; García, F.; Fernández, S.; Guitián, E.; Pérez, D.; Trinquier, G.; Cuniberti, G.; Joachim, C.; Peña, D.; Moresco, F. Dodecacene Generated on Surface: Reopening of the Energy Gap. *ACS Nano* **2020**, *14*, 1011–1017.

(8) Mishra, S.; Lohr, T. G.; Pignedoli, C. A.; Liu, J.; Berger, R.; Urgel, J. I.; Müllen, K.; Feng, X.; Ruffieux, P.; Fasel, R. Tailoring Bond Topologies in Open-Shell Graphene Nanostructures. *ACS Nano* **2018**, *12*, 11917–11927.

(9) Rogers, C.; Chen, C.; Pedramrazi, Z.; Omrani, A. A.; Tsai, H.-Z.; Jung, H. S.; Lin, S.; Crommie, M. F.; Fischer, F. R. Closing the Nanographene Gap: Surface-Assisted Synthesis of Peripentacene from 6,6′-Bipentacene Precursors. *Angew. Chem. Int. Ed.* **2015**, *54*, 15143–15146.

(10) Sánchez-Grande, A.; Urgel, J. I.; Veis, L.; Edalatmanesh, S.; Santos, J.; Lauwaet, K.; Mutombo, P.; Gallego, J. M.; Brabec, J.; Beran, P.; Nachtigallová, D.; Miranda, R.; Martín, N.; Jelínek, P.; Écija, D. Unravelling the Open-Shell Character of Peripentacene on Au(111). *J. Phys. Chem. Lett.* **2021**, *12*, 330–336.

(11) Wang, S.; Talirz, L.; Pignedoli, C. A.; Feng, X.; Müllen, K.; Fasel, R.; Ruffieux, P. Giant Edge State Splitting at Atomically Precise Graphene Zigzag Edges. *Nat. Commun.* **2016**, *7*, 1–6.

(12) Mishra, S.; Yao, X.; Chen, Q.; Eimre, K.; Gröning, O.; Ortiz, R.; Di Giovannantonio, M.; Sancho-García, J. C.; Fernández-Rossier, J.; Pignedoli, C. A.; Müllen, K.; Ruffieux, P.; Narita, A.; Fasel, R. Large Magnetic Exchange Coupling in Rhombus-Shaped Nanographenes with Zigzag Periphery. *Nat. Chem.* **2021**, *13*, 581–586.

(13) Pavliček, N.; Mistry, A.; Majzik, Z.; Moll, N.; Meyer, G.; Fox, D. J.; Gross, L. Synthesis and Characterization of Triangulene. *Nat. Nanotechnol.* **2017**, *12*, 308–311.

(14) Mishra, S.; Beyer, D.; Eimre, K.; Liu, J.; Berger, R.; Gröning, O.; Pignedoli, C. A.; Müllen, K.; Fasel, R.; Feng, X.; Ruffieux, P. Synthesis and Characterization of π-Extended Triangulene. *J. Am. Chem. Soc.* **2019**, *141*, 10621–10625.

(15) Su, J.; Telychko, M.; Hu, P.; Macam, G.; Mutombo, P.; Zhang, H.; Bao, Y.; Cheng, F.; Huang, Z.-Q.; Qiu, Z.; Tan, S. J. R.; Lin, H.; Jelínek, P.; Chuang, F.-C.; Wu, J.; Lu, J. Atomically Precise Bottom-up Synthesis of π-Extended [5]Triangulene. *Sci. Adv.* **2019**, *5*, eaav7717.

(16) Mishra, S.; Beyer, D.; Eimre, K.; Ortiz, R.; Fernández-Rossier, J.; Berger, R.; Gröning, O.; Pignedoli, C. A.; Fasel, R.; Feng, X.; Ruffieux, P. Collective All-Carbon Magnetism in Triangulene Dimers. *Angew. Chem. Int. Ed.* **2020**, *59*, 12041–12047.

(17) Mishra, S.; Xu, K.; Eimre, K.; Komber, H.; Ma, J.; Pignedoli, C. A.; Fasel, R.; Feng, X.; Ruffieux, P. Synthesis and Characterization of [7]Triangulene. *Nanoscale* **2021**, *13*, 1624–1628.

(18) Su, J.; Fan, W.; Mutombo, P.; Peng, X.; Song, S.; Ondráček, M.; Golub, P.; Brabec, J.; Veis, L.; Telychko, M.; Jelínek, P.; Wu, J.; Lu, J. On-Surface Synthesis and Characterization of [7]Triangulene Quantum Ring. *Nano Lett.* **2021**, *21*, 861–867.

(19) Li, J.; Sanz, S.; Castro-Esteban, J.; Vilas-Varela, M.; Friedrich, N.; Frederiksen, T.; Peña, D.; Pascual, J. I. Uncovering the Triplet Ground State of Triangular Graphene Nanoflakes Engineered with Atomic Precision on a Metal Surface. *Phys. Rev. Lett.* **2020**, *124*, 177201.

(20) Mishra, S.; Beyer, D.; Eimre, K.; Kezilebieke, S.; Berger, R.; Gröning, O.; Pignedoli, C. A.; Müllen, K.; Liljeroth, P.; Ruffieux, P.; Feng, X.; Fasel, R. Topological Frustration Induces Unconventional Magnetism in a Nanographene. *Nat. Nanotechnol.* **2020**, *15*, 22–28.

(21) Hu, P.; Wu, J. Modern Zethrene Chemistry. *Can. J. Chem.* **2016**, *95*, 223–233.

(22) Clar, E.; Lang, K. F.; Schulz-Kiesow, H. Aromatische Kohlenwasserstoffe, LXX. Mitteil.[1)]: Zethren (1.12; 6.7-Dibenztetracen). *Chem. Ber.* **1955**, *88*, 1520–1527.

(23) Li, Y.; Heng, W.-K.; Lee, B. S.; Aratani, N.; Zafra, J. L.; Bao, N.; Lee, R.; Sung, Y. M.; Sun, Z.; Huang, K.-W.; Webster, R. D.; López Navarrete, J. T.; Kim, D.; Osuka, A.; Casado, J.; Ding, J.; Wu, J. Kinetically Blocked Stable Heptazethrene and Octazethrene: Closed-Shell or Open-Shell in the Ground State? *J. Am. Chem. Soc.* **2012**, *134*, 14913–14922.

(24) Huang, R.; Phan, H.; Herng, T. S.; Hu, P.; Zeng, W.; Dong, S.; Das, S.; Shen, Y.; Ding, J.; Casanova, D.; Wu, J. Higher Order π-Conjugated Polycyclic Hydrocarbons with Open-Shell Singlet Ground State: Nonazethrene versus Nonacene. *J. Am. Chem. Soc.* **2016**, *138*, 10323–10330.

(25) Zeng, W.; Sun, Z.; Herng, T. S.; Gonçalves, T. P.; Gopalakrishna, T. Y.; Huang, K.-W.; Ding, J.; Wu, J. Super-Heptazethrene. *Angew. Chem. Int. Ed.* **2016**, *55*, 8615–8619.

(26) Zeng, W.; Gopalakrishna, T. Y.; Phan, H.; Tanaka, T.; Herng, T. S.; Ding, J.; Osuka, A.; Wu, J. Superoctazethrene: An Open-Shell Graphene-like Molecule Possessing Large Diradical Character but Still with Reasonable Stability. *J. Am. Chem. Soc.* **2018**, *140*, 14054–14058.

(27) Mishra, S.; Melidonie, J.; Eimre, K.; Obermann, S.; Gröning, O.; A. Pignedoli, C.; Ruffieux, P.; Feng, X.; Fasel, R. On-Surface Synthesis of Super-Heptazethrene. *Chem. Commun.* **2020**, *56*, 7467–7470.

(28) Silva, P. V.; Girão, E. C. Electronic and Transport Properties of Graphene Nanoribbons Based on Super-Heptazethrene Molecular Blocks. *J. Phys. Chem. C* **2021**, *125*, 11235–11248.

(29) Temirov, R.; Soubatch, S.; Neucheva, O.; Lassise, A. C.; Tautz, F. S. A Novel Method Achieving Ultra-High Geometrical Resolution in Scanning Tunnelling Microscopy. *New J. Phys.* **2008**, *10*, 053012.

(30) Gross, L.; Schuler, B.; Pavliček, N.; Fatayer, S.; Majzik, Z.; Moll, N.; Peña, D.; Meyer, G. Atomic Force Microscopy for Molecular Structure Elucidation. *Angew. Chem. Int. Ed.* **2018**, *57*, 3888–3908.

(31) Liu, K.; Qiu, F.; Yang, C.; Tang, R.; Fu, Y.; Han, S.; Zhuang, X.; Mai, Y.; Zhang, F.; Feng, X. Nonplanar Ladder-Type Polycyclic Conjugated Molecules: Structures and Solid-State Properties. *Cryst. Growth Des.* **2015**, *15*, 3332–3338.

(32) Hirao, Y.; Okuda, T.; Hamamoto, Y.; Kubo, T. Formation of Perylenes by Oxidative Dimerization of Naphthalenes Bearing Radical Sources. *ChemPlusChem* **2020**, *85*, 101–109.

(33) Xu, K.; Fu, Y.; Zhou, Y.; Hennersdorf, F.; Machata, P.; Vincon, I.; Weigand, J. J.; Popov, A. A.; Berger, R.; Feng, X. Cationic Nitrogen-Doped Helical Nanographenes. *Angew. Chem. Int. Ed.* **2017**, *56*, 15876–15881.

(34) Gu, Y.; Wu, X.; Gopalakrishna, T. Y.; Phan, H.; Wu, J. Graphene-like Molecules with Four Zigzag Edges. *Angew. Chem. Int. Ed.* **2018**, *57*, 6541–6545.

(35) Ovchinnikov, A. A. Multiplicity of the Ground State of Large Alternant Organic Molecules with Conjugated Bonds. *Theoret. Chim. Acta* **1978**, *47*, 297–304.

(36) Khanna, S. K.; Lambe, J. Inelastic Electron Tunneling Spectroscopy. *Science* **1983**, *220*, 1345–1351.

(37) Hirjibehedin, C. F.; Lutz, C. P.; Heinrich, A. J. Spin Coupling in Engineered Atomic Structures. *Science* **2006**, *312*, 1021–1024.

(38) Li, J.; Sanz, S.; Corso, M.; Choi, D. J.; Peña, D.; Frederiksen, T.; Pascual, J. I. Single Spin Localization and Manipulation in Graphene Open-Shell Nanostructures. *Nat. Commun.* **2019**, *10*, 1–7.

(39) Ternes, M. Spin Excitations and Correlations in Scanning Tunneling Spectroscopy. *New J. Phys.* **2015**, *17*, 063016.